A&A 472, 919–928 (2007)
DOI: 10.1051/0004-6361:20077627
© ESO 2007

Astronomy & Astrophysics

Scattering polarization in strong chromospheric lines

III. Spatial fluctuations of the polarized Ca II K line profiles

R. Holzreuter[1] and J. O. Stenflo[1,2]

[1] Institute of Astronomy, ETH Zentrum, 8092 Zurich, Switzerland
e-mail: holzreuter@astro.phys.ethz.ch
[2] Faculty of Mathematics & Science, University of Zurich, 8057 Zurich, Switzerland
e-mail: stenflo@astro.phys.ethz.ch

Received 10 April 2007 / Accepted 5 June 2007

ABSTRACT

Aims. We explore the spatial variations of the chromospheric Ca II K scattering polarization on the quiet Sun, in particular the fluctuations of the linear polarizations Q/I and U/I, their correlations, varying profile shapes, and center-to-limb variations.
Methods. A set of high precision polarimetric recordings with ZIMPOL (Zurich Imaging Polarimeter) at distinct heliographic positions is used.
Results. Two main effects contribute to the observed fluctuations: (i) Chromospheric magnetic fields (located in the K3 layer), which induce polarization variations via the Hanle effect. (ii) "Hot spots" due to small-scale temperature structuring of the chromosphere, which induce variations of the local scattering geometry. The observed signatures of both effects are influenced by the turbulent broadening, which steeply increases with height, by optical depth variations in the K3 layer, and by the chromospheric temperature stratification. Almost all the fluctuations that are seen with our spatial resolution (approximately 5 arcsec) originate in the high chromospheric K3 layer, while the lower chromospheric layers are much more homogeneous at the resolved scales. The relatively small Q/I fluctuations observed between the K1 and K2 wavelengths constrain the size and lifetime of cold and hot areas in the low and mid chromosphere.
Conclusions. At present it is not possible to disentangle the Hanle effect and the "hot-spot" effect from each other. This would require 2D spatial mapping of the linear polarization at the K3, K2, and K1 wavelengths with higher spatial resolution, which is hard to do with existing telescopes, since the observations are photon starved and require larger telescope apertures.

Key words. line: formation – polarization – scattering – Sun: atmosphere – Sun: chromosphere – Sun: magnetic fields

1. Introduction

In our previous work on the scattering polarization in strong chromospheric lines (Holzreuter et al. 2005, 2006; Holzreuter & Stenflo 2007, henceforth Papers Ia, Ib and II) we have explored the connection between the spatially averaged polarized profile shape with its center-to-limb variation and the radiation-field anisotropy that is governed by the temperature stratification of the atmosphere. We have shown for the Ca II K line that a mixing between a hot and cool atmospheric component is necessary to explain the observational data, and how the hot component gains in relative importance as we approach the solar limb. In the present paper we will turn to the spatial variations along the spectrograph slit of the polarized profiles and explore the magnetic and non-magnetic origins of these variations.

The intriguing asymmetric large scale structure of Ca II H and K seen in the Stokes Q/I spectrum near the solar limb was first observed and explained by Stenflo (1980). In Auer et al. (1980) the first radiative-transfer modeling attempts were made. Saliba (1985) improved the modeling by calculating the Q/I spectrum with a 1D model that accounted for non-LTE populations and partial frequency redistribution (PRD). In Paper Ib we showed that the discrepancy between modeling and observation that was seen in the calculations of Saliba (1985) may be resolved by a superposition of two atmospheric models (i.e. FAL-C of Fontenla et al. (1993) and a much colder model FAL-X, used by Avrett (1995, his model $M_{\rm CO}$)). In Paper II we showed that this superposition produces better results for all the various heliographic positions, although some systematic discrepancies favor scenarios with an increasing relative contribution of the hot component in the higher layers of the chromosphere.

In the present work we use the same data set as in Paper II. This high quality data set, which was obtained with the UV-sensitive ZIMPOL-2 camera system (Gandorfer et al. 2004, and references therein) at Kitt Peak in March 2005, allows us to explore the spatial variations of the features seen around the core region of the Ca II K spectrum. Several of the recorded 2D Stokes spectra of the Ca II K line, which illustrate the spatial variations that we will explore in detail here, have previously been shown and discussed in Stenflo (2006).

2. Data acquisition and reduction

The data acquisition and reduction have been described in detail in Paper II. The ZIMPOL camera has 4×140 available pixels in the spatial direction along the slit, but since three out of each group of four pixel rows are masked to be used as fast buffers for the four image planes (see Gandorfer et al. 2004), the effective number of pixels in the spatial dimension is 140.

Because of the very low intensity of the Ca II K line core, the total integration time for a single observation (composed of the

Article published by EDP Sciences and available at http://www.aanda.org or http://dx.doi.org/10.1051/0004-6361:20077627

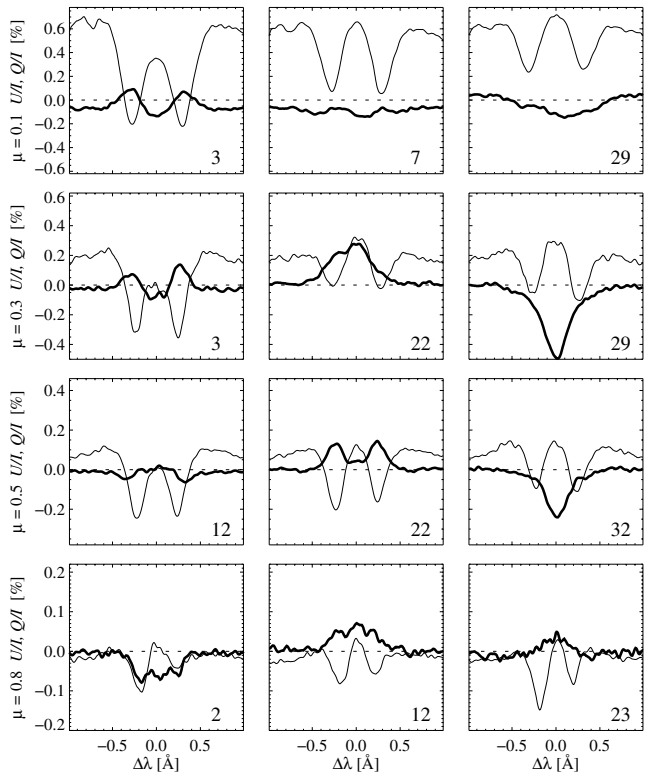

Fig. 1. Selection of Q/I (thin) and U/I (thick) signatures observed along the slit at different heliographic positions μ for a wavelength range of ∓ 1 Å around the line core. The number at the lower right indicates the effective pixel number (in the range 1–35) along the slit. While the global shape of the Q/I spectrum remains qualitatively the same, the U/I profile exhibits interesting variations that can be both positive and negative at either K2 or K3. Note the decreasing polarization scales for increasing μ.

numerical accumulation of many exposures, each of which with an exposure time of about 3 s) was about 5 min. To improve the photon statistics we further did binning of four effective pixels along the spatial dimension, which as a net result gives us 2D images with 770×35 resolution elements covering a range of approximately 5.6 Å times 80 arcsec. Therefore the resolution element in the spatial direction is approximately 2.3 arcsec. We will show that the main structures seen in the spatial direction are much larger. The resolution in the wavelength direction is 7.3 m Å per pixel. In order to optimize the S/N ratio we applied the broadest possible Gaussian spectral smoothing that would not lead to significant degradation of the spectral structures. The chosen full width at half maximum of this Gaussian is 80 mÅ, which is still small in comparison with the width of the structures in the Ca II K core region (cf. Fig. 1, where each tick mark is 100 mÅ). The resulting noise level in the Q/I images is of the order of 0.01%. Since the noise is almost independent of μ (Fig. 3) while the signal increases from about 0.1% at $\mu = 0.8$ to 0.6% at $\mu = 0.1$ (Fig. 1) the S/N-ratio increases accordingly from 10 to 60.

3. Observational features

3.1. Spatial variations

3.1.1. Polarization signatures

In the following we use the abbreviations K1 (weak local Q/I polarization maximum between wing and line core), K2 (distinct minima near the line core) and K3 (line core) for the relevant wavelength positions, as we did in our previous papers. This terminology closely agrees with the one that is used in the literature based on the intensity profile. Note that the absolute wavelength positions may vary with heliographic position or even along the slit for a single spectral recording.

Figure 1 shows the very different behavior of Q/I (thin) and U/I (thick), the two main components of linear polarization produced by scattering. The selection of heliographic positions and spatial locations along the slit illustrates the broad diversity of polarized profile signatures.

The Stokes Q/I spectra show the well-known features near the line core with a polarization maximum at the very line core, distinct minima at K2, and another weak maximum at K1. While the overall structure of the Q/I spectrum is qualitatively preserved for all spectra, and the polarization at K1 is almost constant along the slit for a given μ (the cosine of the heliocentric angle), the variations of the minimum at K2 and the maximum at K3 are considerable. The rather insignificant variations at K1 is likely to be a consequence of the photospheric origin of the line at this wavelength, in contrast to K2 and K3, which are governed by the chromospheric properties.

The observed Stokes U/I signatures vary much more. While zero in the wings outside K1, there are positive or negative contributions at K2 as well as at the line core. Furthermore the signal at K2 seems to be partly uncorrelated with the one at K3 (cf. the three panels for $\mu = 0.3$). Note that the U/I signal can be larger than Q/I and also be of different sign. At first sight there appears to be no obvious correlation between the two components, which can also be taken as convincing evidence for the non-existence of remaining instrumental polarization cross-talk in the data (cf. Paper II for a detailed explanation of the procedure used to eliminate the cross-talk between the Stokes parameters).

The heliographic position has no major influence on the signatures that are seen. The basic Q/I profile shape is conserved for all μ, and the U/I spectrum shows strong variations everywhere. There are no specific features that are only observed at certain heliographic position.

3.1.2. Variation along the slit

The previously described variations of Q/I and U/I are not random when we follow them along the slit for a given spectral recording. Figure 2 shows a continuous section of the slit for $\mu = 0.4$. The series of images shows that the different polarization patterns may coexist at a given heliographic position, and that the transition from one signature to the next takes place on a typical length scale of 4 to 5 resolution elements, corresponding to approximately 10 arcsec.

In the middle part of the panels in Fig. 3 we plot the standard deviation of the two Stokes components along the slit. Both the variations at K3 and at K2 seem to be similar in magnitude for both Stokes parameters. For small μ the variation of the Q/I signal at K2 tends to be slightly larger than the variation of U/I, while the situation at larger μ is ambiguous.

The very small variation of the signal in the wings demonstrates on the one hand the low noise level of the observations and on the other hand the spatially very homogeneous photospheric part of the spectrum. Table 1 lists the FWHM values of Fig. 3. If the variation originates from the Hanle effect, then the wavelength range between the two thin vertical lines would correspond to approximately 6 Doppler widths (since the Hanle effect only operates within ±3 Doppler widths, cf. Stenflo 1998). The corresponding Doppler velocities are also summarized

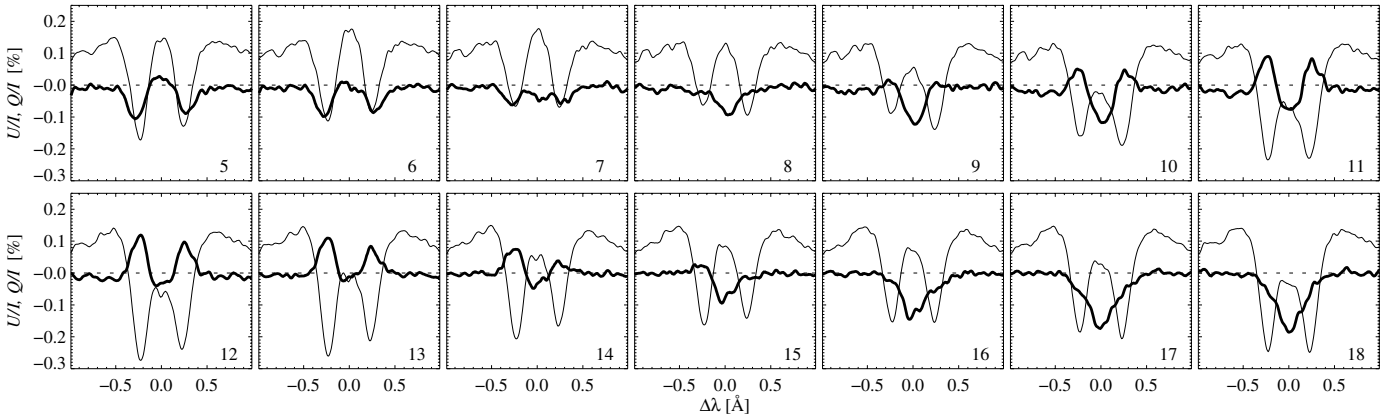

Fig. 2. An example of the variation of the Q/I (thin) and U/I (thick) signals along the slit for $\mu = 0.4$. The number to the lower right of each panel corresponds to the effective, binned pixel number along the slit. The increment between two pixels is 2.3 arcsec. The wavelength range is the same as in Fig. 1. The samples show that for a single heliographic position all the different types of signatures in the Q/I and U/I profiles as in Fig. 1 may be present. The variation along the slit takes place on scales of approximately 10 arcsec.

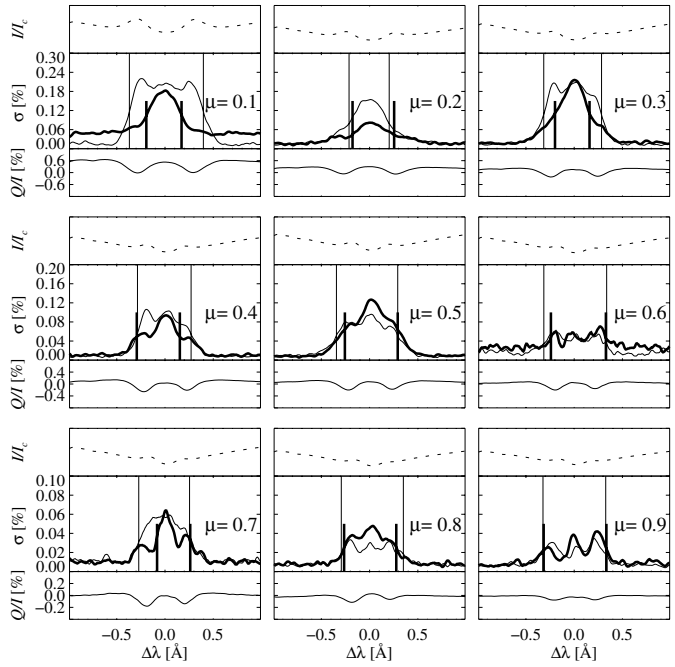

Fig. 3. Standard deviations of the U/I (thick) and Q/I (thin) signals along the slit as functions of wavelength (thick solid) for all nine heliographic positions. The average intensity profile (dotted line in the upper part of the panels) and the Q/I spectrum (thin solid line in the lower part) are given for reference. The wavelength range covered by the panels is identical to that of Figs. 1 and 2. The vertical lines indicate the wavelength positions where the noise-corrected σ ($\sigma_{\rm true}$) of Q/I (thin) and U/I (thick) is at half maximum. $\sigma_{\rm true} = \sqrt{\sigma^2 - \sigma^2_{\rm noise}}$. The noise level is determined in the distant wings, where we assume that $\sigma_{\rm true} = 0$, which implies that $\sigma_{\rm noise} = \sigma$.

in Table 1. Note that due to the odd form of the U/I profiles in Fig. 3 the values at $\mu = 0.4$ and $\mu = 0.7$ are probably too small.

3.1.3. Variation at K2

Figure 4 shows for the first four heliographic positions all the spectra along the slit superposed within each panel. One can clearly see how the invariance at K1 develops into a strong

Table 1. Full width at half maximum of the standard deviation along the slit as plotted in Fig. 3 for Q/I and U/I. The Doppler velocities have been calculated with the assumption that the variation of the polarization is due to the Hanle effect (i.e. covers a range of approximately 6 Doppler widths).

	Q/I		U/I	
μ	*FWHM* [mÅ]	v_D [km s^{-1}]	*FWHM* [mÅ]	v_D [km s^{-1}]
0.1	767.1	9.7	365.3	4.6
0.2	416.8	5.3	431.4	5.5
0.3	599.7	7.6	358.3	4.6
0.4	555.7	7.1	446.0	5.7
0.5	636.1	8.1	548.4	7.0
0.6	650.8	8.2	570.3	7.2
0.7	526.4	6.7	343.6	4.4
0.8	643.4	8.2	541.1	6.9
0.9	650.7	8.3	650.7	8.3

variance at K2 and K3. In the case of $\mu = 0.2$ there are only minor spatial variations, but this rather seems to be an exception (see also Fig. 3). When inspecting Fig. 4, several interesting properties may be noticed:

Firstly, the depths of the minima are correlated with their wavelength positions. The deeper the minimum the closer it is to the line core. Especially the weaker minima tend to be shifted substantially towards the wing. We therefore conclude that the variation of the polarization signal along the slit for a fixed wavelength position is not primarily due to atmospheric motions on scales larger than our resolution element, because such motions would produce a Doppler shift of the spectrum without any direct correlation with the shape of the polarization signatures.

Secondly, the profiles in a single panel hardly intersect. The increase of the polarization from K2 towards line center occurs in nearly the same way for all heliographic positions, such that the various profile curves are almost parallel at these wavelengths. Only the panel for $\mu = 0.3$ shows some significant intersections of the individual profiles. Note that the panels in Fig. 4 may give the wrong impression that the series of profiles represent a sequence along the slit. However, adjacent profile curves are not necessarily adjacent in the spatial direction.

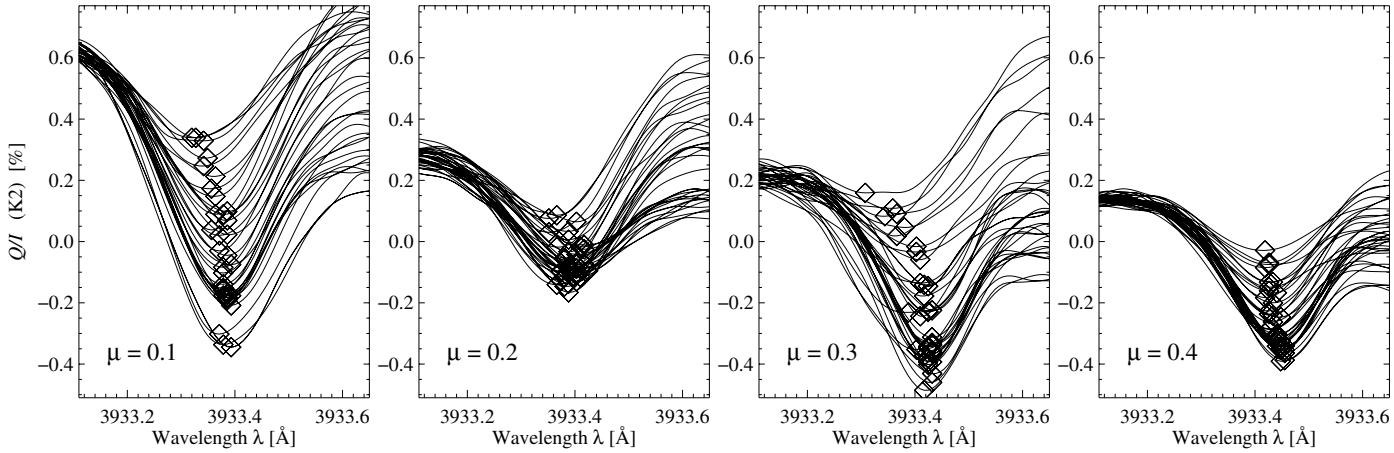

Fig. 4. Position and amplitude of the Stokes Q/I blue-wing minimum at K2 for four different heliographic positions. In each panel all the spectra measured across the slit have been superposed. The K2 minima are marked by diamonds.

Thirdly, the polarization should decrease strongly with increasing μ. At K1 one may see this well-known center-to-limb variation, which has to do with the geometry of the scattering process (see also Paper II). However, the polarization and its variation at K2 does not decrease in the way that one would expect. Note also that the four panels in Fig. 4 have identical scales.

The wavelength position of the K2 polarization minimum correlates not only with its depth but also with the position of the intensity maximum (Stokes I). The scatter plot shown in Fig. 5 includes all the wavelength positions of the Q/I K2 minima and I maxima for the first four heliographic positions. The intensity maximum of K2 is only slightly closer to the line core than the Q/I polarization minimum. The correlation exhibited by Fig. 5 is not surprising, since we have shown in our previous work that both the strength of the K2 polarization minimum and the K2 intensity maximum are directly correlated with the temperature stratification in the lower chromosphere.

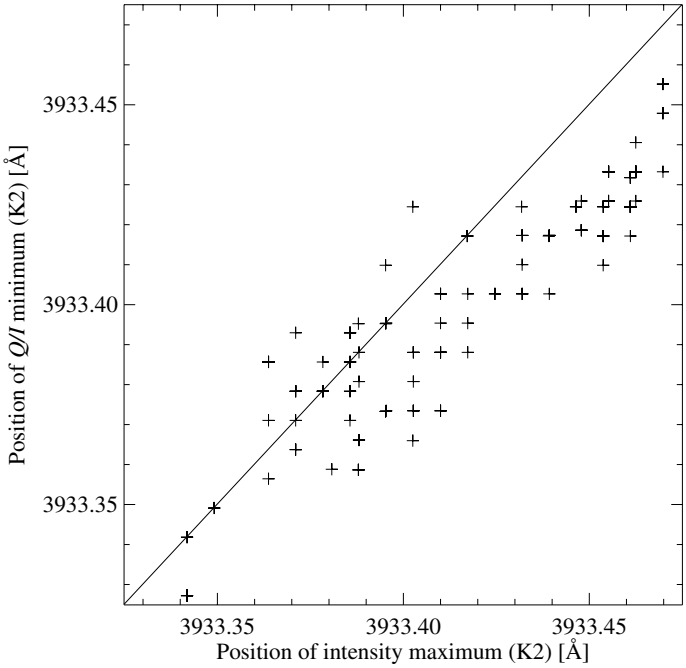

Fig. 5. Position of the polarization minimum in Q/I near K2 versus the position of the corresponding intensity maximum near K2. The plot includes all the points along the slit for the first four heliographic positions (μ = 0.1 to 0.4). Although the variation is not very large in our data, we notice a clear correlation between these two parameters. The position of the Q/I minimum is systematically shifted somewhat towards the wing with respect to the intensity maximum.

3.1.4. Variation at different heliographic positions

The dependence of the variance σ on the center-to-limb distance parameter μ is much weaker than that of the corresponding polarization amplitude. This can be seen in Fig. 6, where the variances of U/I and Q/I along the slit are plotted against μ. For comparison we over-plot the suitably scaled blue wing maximum polarization amplitude in both panels (solid lines). Not shown but very similar is the μ-dependence of the Q/I line core polarization amplitudes. The variance of Q/I along the slit at K3 is the same as that of K2 for all heliographic positions with the exception of $\mu = 0.2$. This is consistent with our findings in the previous section that the individual Q/I spectra hardly intersect between K2 and K3. While the Q/I variance shows some weak μ-dependence, the Stokes U/I variance is even smaller. At K2 we see almost no dependence of the variance with heliographic position. At K3, however, the values are similar to those of Q/I. Note that the recording at $\mu = 0.2$, which does not fit the measurements at other μ in almost every respect, cannot be explained in terms of an erroneously determined μ position. The different behavior of the $\mu = 0.2$ measurement therefore must have its origin in the different physical state of the solar atmosphere in that particular solar region.

3.2. Signal correlations

3.2.1. Correlations between signals at different wavelengths

A surprising correlation in the data is revealed by the scatter plots in Fig. 7, which show strong correlations between the Q/I signals at K3 and K2. For almost all heliographic positions (except $\mu = 0.2$ and $\mu \geq 0.8$, the latter with too low signals to be significant) a simple one to one relation exists (running parallel to the dotted line that represents identical values in the figure). This correlation was already anticipated in Sect. 3.1.3 by our finding that the different spectral profiles along the slit run in parallel between K2 and K3 without intersecting each other. The polarization at K2 is systematically shifted towards lower

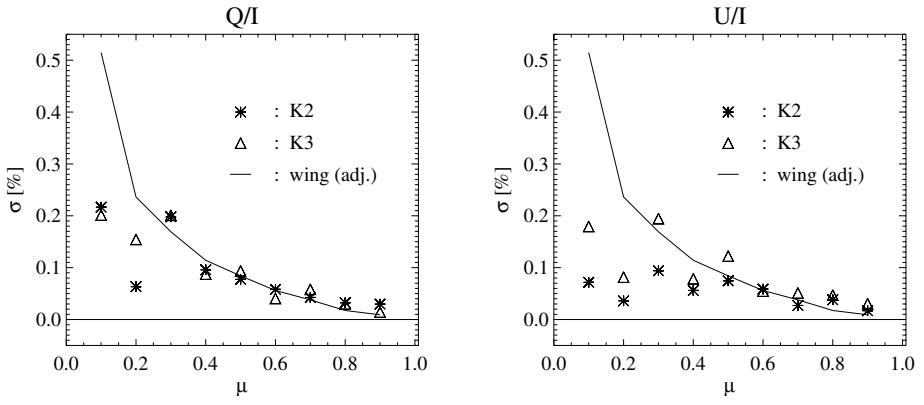

Fig. 6. The spatial variance σ along the slit for Q/I (*left panel*) and U/I (*right panel*) for the two wavelength positions K2 and K3 as functions of μ. The solid lines represent the μ dependence of the Q/I wing polarization (multiplied by an arbitrary scale factor). The size of the symbols corresponds approximately to the size of the error bars.

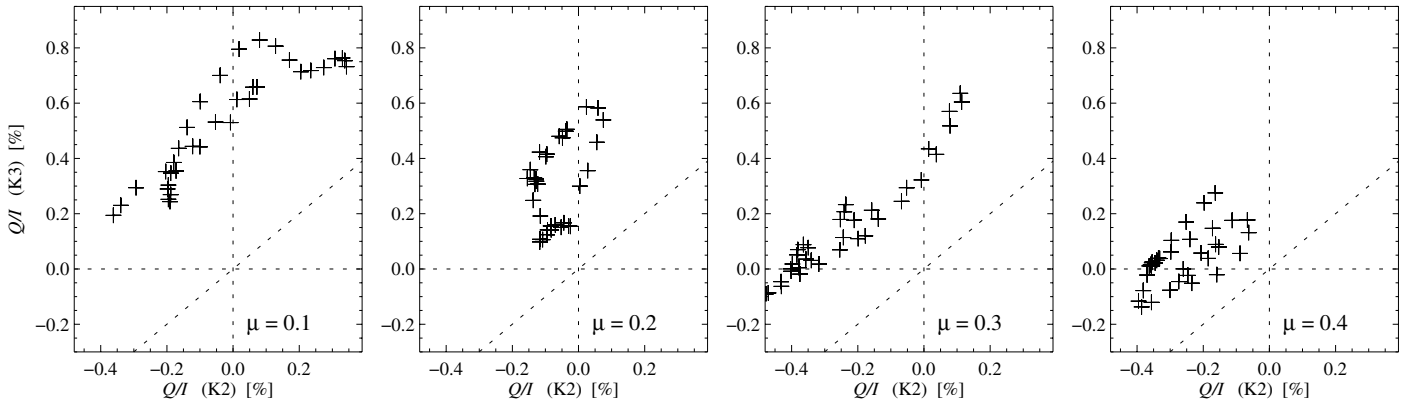

Fig. 7. Stokes Q/I at line center (K3) vs. Q/I at K2 for the first four heliographic positions. The slanted dotted line marks the positions of identical polarization at K2 and K3. The Q/I signal at these two wavelength positions show a surprisingly good correlation (except for $\mu = 0.2$), something that could be anticipated from Fig. 2.

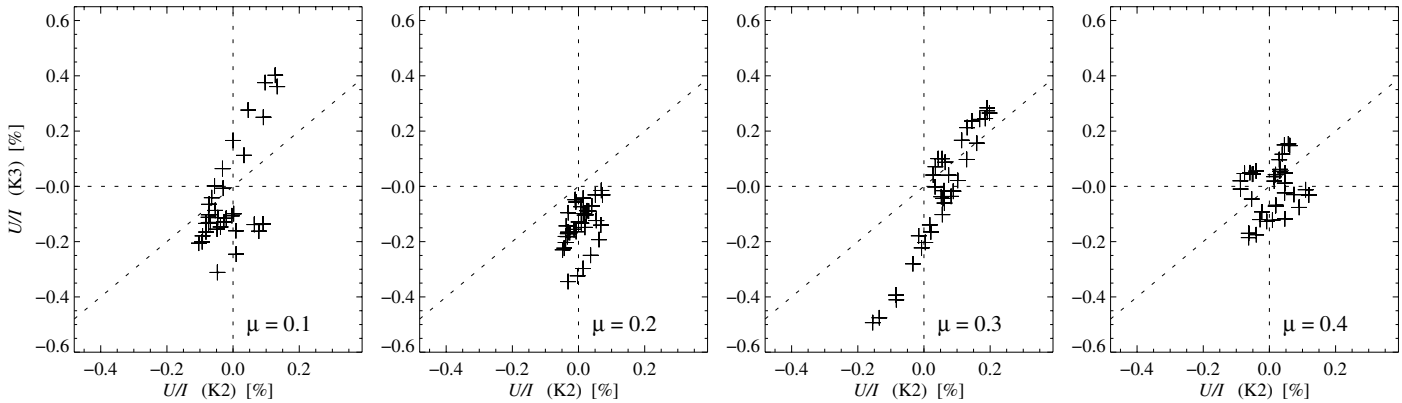

Fig. 8. Same as Fig. 7, but for the Stokes U/I component. Comparison with Fig. 7 shows that U/I is correlated in a similar way, but the slope is different from unity. The variation at K2 is much weaker than at K3, and several recordings show no correlation at all (in particular at $\mu = 0.2$ and $\mu = 0.4$). The polarization range for both axes is the same in all the plots of Figs. 7 and 8.

values, which is related to the triplet profile shape with a K3 maximum surrounded by K2 minima, which in turn has to do with the chromospheric temperature structure. However, as K2 and K3 are formed at different heights, we would not have expected that there would be such a close correlation between the K2 and K3 polarizations. Furthermore, the observed correlation persists also for all the not plotted heliographic positions.

If there is a strict correlation between the Q/I amplitudes at K2 and K3, one would expect a similar behavior of U/I as well. Figure 8 shows the corresponding scatter plot for U/I with the same scales as in Fig. 7 (apart from a small shift of the y-axis to achieve better centering of the pattern in the panels). We notice that a correlation between K2 and K3 exists also for U/I, but it is much weaker. The variation at K2 is smaller by at least a factor of two. For certain heliographic positions there is no correlation at all or even an anti-correlation (see also the images in Stenflo 2006, which show portions of the same data set).

Another weaker correlation exists between the Q/I maximum at K3 and the strength and width of the K2 intensity maximum (see e.g. the right panel of Fig. 3 in Stenflo 2006). It seems that with increasing width of the intensity line core one gets increasing positive polarization contributions from the line core into the K2 polarization minima. The influence of the K3 line

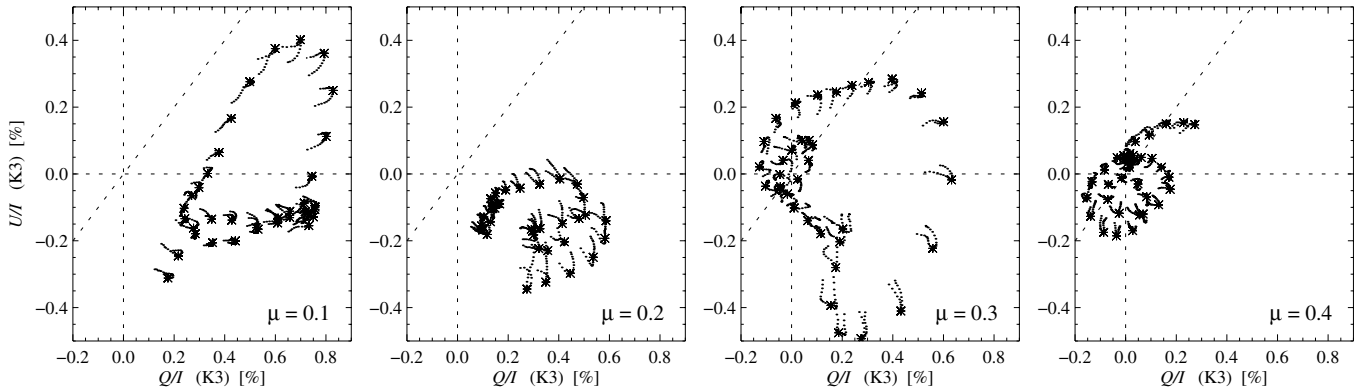

Fig. 9. Correlation between U/I and Q/I along the slit at line center (K3) for the same heliographic positions as in Figs. 7 and 8. The stars refer to the polarization values at the exact K3 wavelength, while the small dots refer to neighboring wavelengths, to give an impression of the degree of variation in the wavelength direction. The most conspicuous pattern is the circular variation of the polarization from large Q/I to large U/I and vice versa.

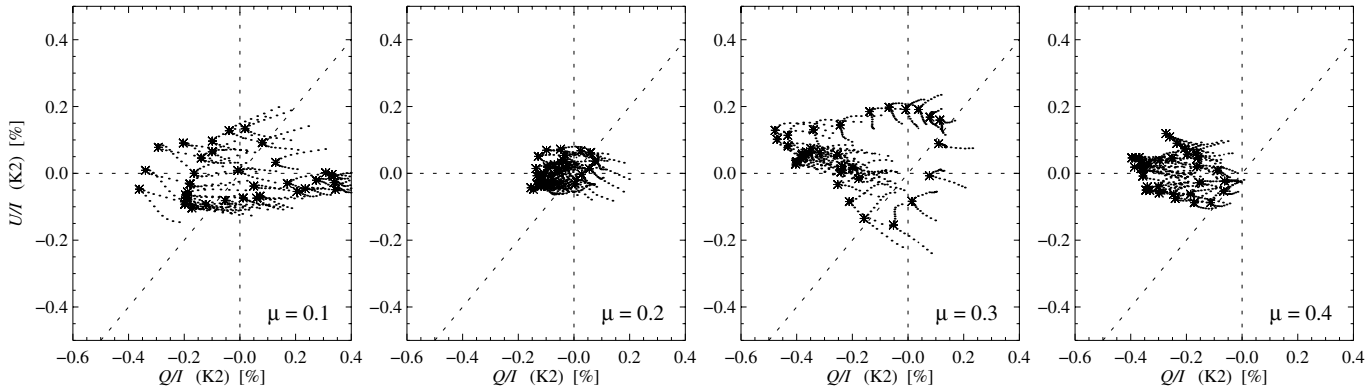

Fig. 10. Correlation between U/I and Q/I as in Fig. 9, but for the individual K2 wavelengths (i.e. at the K2 Q/I minima). Although the correlation pattern is similar to the one at K3, the variation is significantly smaller at K2, and the circular features seen in Fig. 9 are much less dominant.

core thus tends to spread out into K2 and even beyond. This is consistent with the correlations revealed by Fig. 7.

3.2.2. Correlations between Q and U

As already seen in the examples given by Figs. 1 and 2 there appears to be no obvious correlation between the Q/I and the U/I spectra. In the scatter plots of Figs. 9 and 10, however, a certain degree of correlation between these two Stokes parameters may be seen at both K3 and K2. A pattern indicating a rotation of the polarization plane from Q/I to U/I and vice versa is found for $\mu = 0.1$, $\mu = 0.3$ and $\mu = 0.5$ (not shown). This shows that the symmetry-breaking mechanism on the Sun changes gradually from one spatial location to the next. It is not clear whether the symmetry breaking that causes this rotation of the polarization plane is due to gradually varying magnetic fields (via the spatially resolved Hanle effect) or to brightness inhomogeneities (local "hot spots") in the atmosphere. Figure 10 shows that the correlation between Q/I and U/I is much weaker at K2 than in the line core (K3).

4. Interpretation

In the previous section we have extracted a number of interesting properties of the polarized spectra. When we now focus on the interpretation we are particularly interested in the origin of the strongly varying signatures of Q/I and U/I at K2 and K3. In particular we want to explore how the Q/I profile, which we previously used (cf. Paper II) to diagnose the temperature stratification, is influenced by other factors than the temperature, and we would like to determine how much of the variations near the line core may be attributed to magnetic fields via the Hanle effect.

To aid the subsequent discussion we introduce the following abbreviations: To relate a given parameter to a certain wavelength position we use upper indices with parentheses, e.g. $Q/I^{(\mathrm{K2})}$ or $U/I^{(\mathrm{K1})}$. For the spatial variance along the slit we use the Greek letter σ with the same wavelength indices as specified before, while we use lower indices to denote the Stokes parameter that is considered. Thus $\sigma^{(\mathrm{K3})}_{Q/I}$ denotes the standard deviation, i.e. the spatial variance of Q/I along the slit at the line core.

To explain the observed properties of the polarized spectra, one needs to consider the following main factors that affect the scattering polarization:

1. The *temperature stratification*. As discussed in our previous work (Papers Ia, Ib and II) and in Trujillo Bueno (2003), the temperature and density stratifications near the boundary of the atmosphere are responsible for the anisotropy of the radiation field. In a 1D atmosphere without magnetic fields only Stokes Q/I is produced. The polarization varies steeply with center-to-limb distance.
2. *Local inhomogeneities*. Deviations from the plane-parallel symmetry of the atmosphere may produce U/I polarization.

In the absence of magnetic fields the amplitude of Stokes U/I may therefore serve as a measure of the spatial inhomogeneity of the atmosphere at the resolved spatial scales. A hot spot in the atmosphere may for instance produce locally anisotropic illumination of the scattering atom, which results in a rotation of the plane of polarization depending on the relative positions of the atom, the hot spot, and the line of sight. If the position of such a hot spot is random, the produced U/I signal will also be random and hardly μ-dependent.

3. *Magnetic fields*. Another possibility to break the symmetry of the scattering system is through weak magnetic fields, which may rotate the plane of polarization through the Hanle effect. If the fields are spatially resolved we may observe a net U/I signature caused by the Hanle effect. Turbulent magnetic fields rotate the plane of polarization in random directions, such that the U/I rotation contributions may cancel out completely if the turbulent field elements are not spatially resolved (e.g. Stenflo 1982; Faurobert-Scholl 1992; Stenflo et al. 1998; Bianda et al. 1999; Trujillo Bueno 2001; Berdyugina & Fluri 2004). Therefore unresolved turbulent magnetic fields only decrease an already existing Q/I polarization signal, while resolved fields may produce signatures in both Q/I and U/I.

With this background we will now go through the observed features described in the previous section and try to identify which cause could potentially be responsible for each of them, and which conclusions can be drawn. The following list summarizes the most important observational properties:

(1) The overall Q/I profile is characterized by an extended wing and the typical K1 broad maximum – K2 minimum – K3 maximum triplet structure. The signal amplitude decreases rapidly with increasing μ. $U/I^{(\mathrm{wing})}$ and $U/I^{(\mathrm{K1})}$ are always zero.
(2) $Q/I^{(\mathrm{K2})}$ shows considerable variations along the slit, while $\sigma^{(\mathrm{K1})}_{Q/I}$ is small. In particular for small μ, positions along the slit exist where $Q/I^{(\mathrm{K2})}$ can be either positive or negative.
(3) The wavelength position of the $Q/I^{(\mathrm{K2})}$ minimum correlates with its depth. Weaker minima are systematically shifted away from the core.
(4) $Q/I^{(\mathrm{K2})}$ is closely correlated with $Q/I^{(\mathrm{K3})}$ for almost every μ position. $\sigma^{(\mathrm{K2})}_{Q/I}$ therefore equals $\sigma^{(\mathrm{K3})}_{Q/I}$.
(5) Non-zero Stokes U/I values occur only in an extended core region out to a wavelength somewhere between K1 and K2.
(6) $U/I^{(\mathrm{K2-K3-K2})}$ sometimes has the same profile shape as $Q/I^{(\mathrm{K2-K3-K2})}$ (although it may be of both the opposite or the same sign). At other places $U/I^{(\mathrm{K2-K3})}$ has a completely different shape (e.g. a single peak instead of a triplet structure).
(7) The absolute U/I polarization amplitude may be larger than the corresponding Q/I amplitude.
(8) $U/I^{(\mathrm{K3})}$ and $Q/I^{(\mathrm{K3})}$ show a correlation that corresponds to a gradual rotation of the plane of polarization along the slit. At K2 this correlation is weaker.
(9) $U/I^{(\mathrm{K3})}$ is only weakly (and not always) correlated with $U/I^{(\mathrm{K2})}$. The slope of the regression line differs from unity. $\sigma^{(\mathrm{K2})}_{U/I}$ is smaller than $\sigma^{(\mathrm{K3})}_{U/I}$ for small μ (close to the limb).
(10) The variance σ has a shallower μ dependence than the polarization amplitudes. In particular $\sigma^{(\mathrm{K2})}_{U/I}$ is almost independent of heliographic position.

Various physical mechanisms contribute in different ways to each of these ten properties. Our next task is to try to identify these mechanisms and the roles they play.

4.1. Temperature stratification

Let us start with a discussion of properties (1) and (2), which only relate to Q/I but not to U/I. We may therefore attempt to interpret them in terms of the atmospheric stratification. The overall Q/I polarization signature (property (1)) can be fully explained by standard 1D models, as we have done in Papers Ia, Ib and II. The Q/I polarization in the core region is reproduced by 1D models with a moderate chromospheric temperature rise or with a two-component model consisting of a hot and a cold component.

The observed variances $\sigma^{(\mathrm{K2})}_{Q/I}$ and $\sigma^{(\mathrm{K1})}_{Q/I}$ are much smaller than the difference between the Q/I values that result from the hot and cold 1D atmospheres used in Papers Ib and II. To obtain a fit between the observations and 1D modeling of K1 and K2, only small adjustments of the chromospheric temperature stratification are needed. Variations of this stratification would however also generally give rise to a $\sigma^{(\mathrm{K1})}_{Q/I} > 0$, which would be in contradiction with our observations. Therefore either the spatial variation of the temperature in the atmospheric layer where K1 is formed is much smaller than in the K2 layer, or it occurs on smaller spatial or shorter temporal scales than our present resolutions (spatially about 5 arcsec when accounting for seeing, temporally as determined by our 5 min integration time). Neither possibility can be ruled out. We are however able to rule out resolved long lasting large volumes of cold or hot plasma (cold and hot with respect to the standard atmospheres used in Papers Ib and II) in the quiet Sun at heights up to the K2 layer.

4.2. Macroscopic motions, turbulent broadening, and optical thickness variations

Let us here note that one needs to distinguish between the K2/K3 wavelengths and the corresponding K2/K3 layers in the atmosphere. The wavelength positions denote specific places in the spectrum, which are approximately but not strictly formed in the corresponding atmospheric layer. In the following discussion it is important to understand that sometimes fluctuations in the K3 layer can be responsible for variations at K2 wavelengths.

Properties (3) and (4) may be explained in terms of turbulent Doppler broadening. In Paper II we showed that enhanced turbulence in the K2 and K3 layers leads to shallower K2 minima and a wavelength shift towards the wings, very similar to property (3) that we have found. The generally accepted picture of the chromosphere is that it is weakly turbulent in its lower part (the K2 layer between 500 km (the classical temperature minimum) and 1500 km above $\tau = 1$) and has an increasingly turbulent upper part (the K3 layer above 1500 km). However, the exact 1:1 correlation of property (4), which is also observed at all other μ, and the weaker correlation of property (9), are not expected from this explanation.

Macroscopic atmospheric motions may produce significant wavelength shifts of the spectral profiles. If such Doppler shifts were the cause of the Q/I variance, then we would expect the magnitude of the variance to scale with the wavelength gradient of the Q/I profile. In contradiction to this expectation we find however that the variation of the polarization along the slit is largest at wavelengths (e.g. at K2) with a small wavelength

gradient of Q/I (see Fig. 3). We can therefore rule out macroscopic motions as a cause for the observed variance.

Alternatively, a variable optical thickness of the K3 layer could be the cause of the variations along the slit, because the K3 layer usually contributes to a positive Q/I, while the K2 layer mainly produces negative contributions (cf. Paper Ib). The linear correlation between $Q/I^{(\mathrm{K2})}$ and $Q/I^{(\mathrm{K3})}$ would then have a consistent explanation if the K3 layer gives a broad contribution over a range that includes K2 (but not K1). In this case the K2 layer may not exhibit its own variations along the slit to its full extent. This requires strong density variations at the K3 layer or the Doppler width in this layer must – at least temporarily – be very large (at least of order 20 $\mathrm{km\,s^{-1}}$). Note that strong $Q/I^{(\mathrm{K3})}$ polarization is often seen together with a broadening of the K2 intensity maxima, which supports the conjecture of density variation or large-amplitude motions in the K3 layer.

4.3. Hanle effect or local "hot spots"?

4.3.1. Limitation to the core region

The mere existence of $U/I^{(\mathrm{K1-K2})}$ polarization, property (5) above, can only be explained in terms of symmetry breaking either by deviations from spherical symmetry of the atmospheric stratification (e.g. by local "hot spots"), or by magnetic fields via the Hanle effect.

To distinguish between these two alternative origins one may want to make use of the well-known property of the Hanle effect that it can only operate within a limited wavelength range, ±3 Doppler widths around the line center, as assumed in Table 1. The shapes of the two $\sigma(\lambda)$ profiles in Fig. 3 are rather rectangular, as expected for the Hanle effect. However, the apparent Hanle profile as determined by us by computing $\sigma(\lambda)$ is effectively the result of a sum over profiles that originate at all contributing heights in the atmosphere. Each contribution from a given height is a product of the theoretical and almost rectangular Hanle profile and the strength of the magnetic field. As the Doppler width (which governs the width of the Hanle profile) and the magnetic field strength are height-dependent, the composite net profile may be a complicated mixture of significantly different contributions. From standard atmospheric models one expects the Doppler width to increase with height while the magnetic field strength would decrease with height. One also needs to remember that Stokes U/I can only be produced by spatially resolved magnetic fields, while Q/I is also sensitive to spatially unresolved mixed-polarity fields.

The values for the Doppler velocities derived from Fig. 3 and listed in Table 1 are large but not outside the observed range (Mein et al. 1987). The smaller Doppler width in the K2 layer (as used in the calculations done in Paper Ib) could be masked by the larger velocities and therefore a much larger optical depth of the K3 layer above it. In this case $U/I^{(\mathrm{K2})}$ may be predominantly caused by the Hanle effect in the K3 layer due to the larger turbulence velocities.

Although these arguments about the profile shape of the polarization variance speak in favor of the Hanle effect, one can also make a reasonably compelling case for an interpretation in terms of "hot spots" that produce local variations of the anisotropies of the radiation field. A nearly rectangular profile for the standard deviation of the U/I and Q/I polarizations may result because of the height dependence of the degree of homogeneity of the atmosphere. While the photosphere is very homogeneous at our present spatial and temporal resolutions, the chromosphere is very inhomogeneous. Therefore at the K1 wavelength, for which the spectrum is formed at or slightly above the classical temperature minimum, no U/I polarization would be expected from local inhomogeneities, since spatially resolved hot spots at that height do not exist with significant amplitude. The hot-spot effect will only be effective closer to the line center, because the radiation there originates from higher layers in the atmosphere, where the local inhomogeneities become sufficiently significant to break the spherical symmetry. This leads to almost the same wavelength profile for the polarization variance as for the Hanle effect.

4.3.2. *U* and *Q* correlations

At the locations along the slit where the $U/I^{(\mathrm{K2-K3-K2})}$ pattern has a similar shape as the $Q/I^{(\mathrm{K2-K3-K2})}$ pattern, property (6) may appear to suggest that U/I is there produced by the Hanle effect due to a spatially resolved field that has the same strength and direction in both the K2 and the K3 layers. This is however unlikely, because the Doppler width in the K2 layer is estimated to be too small. Other slit locations where the Q/I and U/I patterns are different make an explanation in terms of the Hanle effect more complicated and therefore a bit contrived. In these cases one would need a magnetic field configuration that changes its direction between the K2 and K3 layers, which may not be excluded but is probably not very likely. From the sign reversal in property (2) and from property (7) – in particular at small μ – the interpretation in terms of a spatially resolved Hanle effect encounters another hurdle: At limb positions where the Q/I polarization is already strong, it can hardly be transformed into an even stronger U/I polarization. As a consequence of the rotation of the plane of polarization to produce a strong U/I, the Q/I polarization should be significantly reduced.

Property (8) also supports an interpretation in terms of varying anisotropy conditions ("hot spots") in the radiation field. The slow rotation from Q to U and back that we see at K3 and to a less extent also at K2 could, in case of the Hanle effect, only be explained by rather homogeneous magnetic fields that exhibit a gradual rotation as we move along the slit, but it is questionable how likely such structures are in the low chromosphere of the quiet Sun. An alternative, appealing interpretation is that there is a hot spot near the slit, which gradually rotates the anisotropy when moving along the slit, since the different points along the slit see the hot spot from different angles. The weaker correlation at K2 due to the greater homogeneity of the K2 layer implies that the hot spots mainly occur in the higher K3 layer.

On the other hand, the weaker correlation between $U/I^{(\mathrm{K3})}$ and $U/I^{(\mathrm{K2})}$, property (9), may easily be explained in terms of the Hanle effect if we as before assume that the polarization variance that is seen at the K2 wavelengths originates in the K3 rather than in the K2 layer. The weaker correlation found in U/I may then be related to the different response of the Hanle effect to resolved fields and unresolved mixed-polarity fields. At the K3 wavelengths we are near the line center where the Doppler velocities are small, which favors contributions from larger-scale structures that are not tangled up by the motions. At the K2 wavelengths on the other hand the Hanle scattering selectively has to involve high velocity atoms in the K3 layer to make the scattered photons appear as far from the line center as K2. Large velocities are more likely to be associated with strong turbulence, which would tangle up the field and thus wipe out the Hanle-induced U/I. For a non-magnetic explanation in terms of the hot spot alternative, we recall that the μ-dependent Q/I polarization is primarily determined by the spherically symmetric component of the vertical stratification of the atmosphere, while

Stokes U/I is affected by azimuthal inhomogeneities (our "hot spots"). The different correlations could then be explained by a height increase of the azimuthal inhomogeneity (more hot spots in the K3 than in the K2 layer). However, the reduced wavelength width of the $\sigma_{U/I}$ profile as compared with $\sigma_{Q/I}$ when we go to smaller μ appears to contradict this explanation, because at small μ the radiation comes from higher regions of the atmosphere, and therefore larger atmospheric fluctuations would be expected.

Property (10) that is based on Fig. 6 gives some insight into the different contributions. The variance of U/I should not be μ-dependent if it is due to local temperature inhomogeneities. $\sigma_{U/I}^{(\mathrm{K2})}$ is indeed found to be almost independent of heliographic position. This is an indication that no spatially resolved Hanle effect takes place at the K2 wavelengths, but that instead the atmospheric inhomogeneities are responsible for the observed variance in $U/I^{(\mathrm{K2})}$. Note, however, that this variance is small as compared with the variance of U/I at K3, or the variance of Q/I. The variance $\sigma_{U/I}^{(\mathrm{K3})}$ is generally larger than $\sigma_{U/I}^{(\mathrm{K2})}$ and shows dependence on heliographic position, which indicates an origin in terms of the spatially resolved Hanle effect. Therefore $U/I^{(\mathrm{K3})}$ is at least partly caused by resolved magnetic fields. A Hanle interpretation of $U/I^{(\mathrm{K3})}$ implies that also $Q/I^{(\mathrm{K3})}$ is affected, and, in combination with property (4), that $Q/I^{(\mathrm{K2})}$ is affected as well. The magnitude of the fluctuations and their μ dependence are similar for $U/I^{(\mathrm{K3})}$ and $Q/I^{(\mathrm{K3})}$, which leads to the conclusion that the turbulent Hanle effect on $Q/I^{(\mathrm{K3})}$ is small. Figure 6 shows however that the variance is much less μ dependent than the wing or line core Q/I polarization, which is an indication that non-magnetic local inhomogeneities may also be a relevant contributor.

4.3.3. Summary: Hanle effect *and* local "hot spots"!

In summary we note that it is difficult to disentangle the Hanle effect from the effect of local hot spots in chromospheric observations. The surprising properties (4) and (9) pose puzzling questions, which may be explained in terms of large Doppler velocities in combination with both resolved and and spatially unresolved turbulent fields. The varying μ dependence of the variance σ also indicates a major role of Hanle effect. On the other hand the large Doppler velocities needed in the K2 layer as well as the properties (2), (6), (7), and (8) all suggest that local inhomogeneities of the chromospheric radiation field are a more likely source of the observed U/I signatures. We believe that the explanation has to involve a complex combination of the various factors, with significant contributions from both the Hanle effect and local hot spots. Anisotropy variations (hot spots) can hardly be the only cause, because magnetic fields are omnipresent and therefore the Hanle effect must always play a significant role. The Hanle effect can be either due to spatially resolved fields or to unresolved, mixed-polarity turbulent magnetic fields, but most likely it is due to a combination of both. On the other hand the Hanle effect can hardly be the sole cause, because high-contrast temperature structuring of the chromosphere (implying abundant local "hot spots") are evident in every Ca II H/K or Hα image.

Let us finally note that our $\mu = 0.2$ recording seems to be an exception which does not conform well to the behavior of the rest of the data, since for this recording $\sigma_{Q/I}^{(\mathrm{K2})}$ is very small and $U/I^{(\mathrm{K2})}$ is zero. Under the assumption that the K3 layer usually is the source of the variance of $Q/I^{(\mathrm{K2})}$, this particular recording seems to represent a moment of very quiet Sun with reduced turbulence in the K3 layer. This suggests that the variation seen at K2 in this specific case is mainly due to variations in the K2 layer itself. The vanishing $U/I^{(\mathrm{K2})}$ suggests that we in this case do not have any spatially resolved Hanle effect at the K2 wavelength. However, this non-conforming case demonstrates that our present data set does not represent a sufficiently big statistical sample, more observations, if possible with better spatial and temporal resolutions, are needed.

5. Concluding remarks

Our analysis of the spatial variations of the Stokes parameters along the slit and with center-to-limb distance have given us insight into the complex and interconnected physical mechanisms that contribute to the formation of the polarized Ca K line profiles. These fluctuations contain convolved information on the physical conditions in the chromosphere, including the chromospheric magnetic fields. The present work is a first step to indicate what it takes to untangle this information.

One fundamental distinction that one must make is between the resolved and unresolved scale domains. In our data the division line between these two scales lies around 5 arcsec spatially (including the estimated seeing effects) and 5 min temporally. At the resolved scales the line wings and the wavelengths around K1 (formed in the upper photosphere and around the temperature minimum) show no significant variations of the Stokes parameters along the slit. The 1D atmospheric models that we have used in our previous papers (cf. in particular Paper II) are therefore still valid. They include a colder temperature minimum combined with a moderate temperature rise in the chromosphere. We show that the variations seen in our observations do not have their origin in the temperature stratification of the low chromosphere, which seems to be homogenous on our resolved scales. However, we also know from Paper II that a spatially unresolved mixture of 1D colder and hotter components are needed to simultaneously fit both the intensity profiles and the polarization profiles for all heliographic positions. It is not yet clear how good the approximation with a 1D mixture is, and how much multidimensional radiative transfer (which would be computationally very expensive) would change the picture.

The conclusion about the temperature homogeneity of the K1 layer at our present resolution also applies to the K2 layer, although at first sight the fluctuations at the K2 wavelength appear significant in comparison with those at the K1 wavelength. However, the observed strict proportionality between the fluctuations at the K2 and K3 wavelengths indicates that the fluctuations seen at K2 are not due to temperature variations in the K2 layer but to the varying contributions from the K3 layer. This implies that the residual variations in the K2 layer should be very small. However, even if this interpretation is not fully valid, 1D model calculations with temperature fluctuations in the K2 layer suggest polarization fluctuations that are at least three times larger than the observed ones, which again supports the interpretation that the K2 layer is indeed quite homogeneous.

The distinction between the resolved and unresolved domains is also crucial in the context of the Hanle effect. Spatially unresolved magnetic fields give Hanle signatures that easily cancel out in U/I (Hanle rotation) while not canceling out in Q/I (Hanle depolarization). Another trademark of the Hanle effect is that it is limited to a core region of ±three Doppler widths. Since the Doppler width in the chromosphere is mainly determined by the turbulent motions, the Hanle signatures are coupled to the turbulent broadening, which increases strongly with height. Only in the K3 layer can we expect Doppler velocities that are large enough for the Hanle effect to be able to show

up at K2 wavelengths. The K3 chromospheric layer shows a large amount of structuring at the scales that we resolve, in contrast to the other, lower-lying layers. As this structuring is seen also in the intensity spectra, it involves not only magnetic fields but also temperature fluctuations. Due to the spectral width of the K3 contributions, they also extend to the K2 wavelengths. Fluctuations of the K3 opacity may therefore induce spectral fluctuations at K2.

The observed, spatially resolved fluctuations in Q/I and U/I can be explained both in terms of the Hanle effect from resolved magnetic fields and from the varying local scattering geometry due to hypothetical K3 "hot spots" located to the side of the slit position (such that the illumination angle varies as we move along the slit). We have presented arguments why this is not an "either-or case", but that both these effects contribute significantly to the fluctuations that we see in our data. For unambiguous, quantitative diagnostics we need to be able to disentangle these two effects from each other, which is a challenging though doable task.

To advance towards such disentanglement future observations need to improve in two main respects: (i) We need to spatially map the fluctuations of the Stokes parameters, for instance by using a tunable narrow-band filter for the Ca K line that can produce both intensity and polarized images at the K3, K2, and K1 wavelengths. (ii) The current spatial and temporal resolutions need to be dramatically improved, to allow us to identify the hot spots and other structures that may play a role in determining the local scattering geometry. This may in principle allow us to isolate the geometry effects from the magnetic field effects and thereby enable us to determine the strengths and orientations of the chromospheric magnetic fields. Since however there is a direct tradeoff between spatial and temporal resolution on the one hand and polarimetric noise on the other hand, we are in a photon-starved regime and therefore need telescopes with larger photon-collecting apertures than currently available telescope systems.

Acknowledgements. A. Feller, C. Thalmann, D. Gisler, M. Bianda, R. Ramelli, A. Gandorfer, and C. Keller helped to obtain the outstanding observational data used in this work. R.H. deeply appreciates the tolerance and flexibility of Prof. Dr. Norbert Dillier concerning the working hours in the department of Otorhinolaryngology, Head and Neck Surgery at the University Hospital of Zurich. We thank the referee for his constructive suggestions which helped us to improve our manuscript.

References

Auer, L. H., Rees, D. E., & Stenflo, J. O. 1980, 88, 302
Avrett, E. H. 1995, in Infrared tools for Solar Astrophysics: What's Next, ed. J. R. Kuhn, & M. J. Penn, NSO/SP Summer Workshop, NSO, Sunspot, 303
Berdyugina, S. V., & Fluri, D. M. 2004, 417, 775
Bianda, M., Stenflo, J. O., & Solanki, S. K. 1999, 350, 1060
Faurobert-Scholl, M. 1992, 258, 521
Fontenla, J. M., Avrett, E. H., & Loeser, R. 1993, 406, 319
Gandorfer, A. M., Povel, H. P., Steiner, P., et al. 2004, A&A, 422, 703
Holzreuter, R., & Stenflo, J. O. 2007, 467, 695
Holzreuter, R., Fluri, D. M., & Stenflo, J. O. 2005, 434, 713
Holzreuter, R., Fluri, D. M., & Stenflo, J. O. 2006, 449, L41
Mein, P., Mein, N., Malherbe, J. M., & Dame, L. 1987, 177, 283
Saliba, G. J. 1985, 98, 1
Stenflo, J. O. 1980, 84, 68
Stenflo, J. O. 1982, 80, 209
Stenflo, J. O. 1998, 338, 301
Stenflo, J. O. 2006, in Solar Polarization, Proc. 4th SPW, ed. R. Casini, & B. W. Lites, ASP Conf. Ser., 358, 215
Stenflo, J. O., Keller, C. U., & Gandorfer, A. 1998, 329, 319
Trujillo Bueno, J. 2001, in Advanced Solar Polarimetry – Theory, Observations, and Instrumentation, ed. M. Sigwarth, ASP Conf. Ser., 236, 161
Trujillo Bueno, J. 2003, in Solar Polarization, Proc. 3rd SPW, ed. J. Trujillo Bueno, & J. Sánchez Almeida, ASP Conf. Ser., 307, 407